Journal of Colloid and Interface Science 650 (2023) 1821–1832

Contents lists available at ScienceDirect

Journal of Colloid And Interface Science

journal homepage: www.elsevier.com/locate/jcis

Carrier peptide interactions with liposome membranes induce reversible clustering by surface adsorption and shape deformation

Ragna Guldsmed Diedrichsen [a], Valeria Vetri [b], Sylvain Prévost [c], Vito Foderà [a], Hanne Mørck Nielsen [a,*]

[a] Center for Biopharmaceuticals and Biobarriers in Drug Delivery (BioDelivery), Department of Pharmacy, University of Copenhagen, Universitetsparken 2, 2100 Copenhagen, Denmark
[b] Department of Physics and Chemistry, University of Palermo, Viale delle Scienze Ed. 18, 90128 Palermo, Italy
[c] Institut Laue-Langevin, 71 avenue des Martyrs, 38042 Grenoble Cedex 9, France

GRAPHICAL ABSTRACT

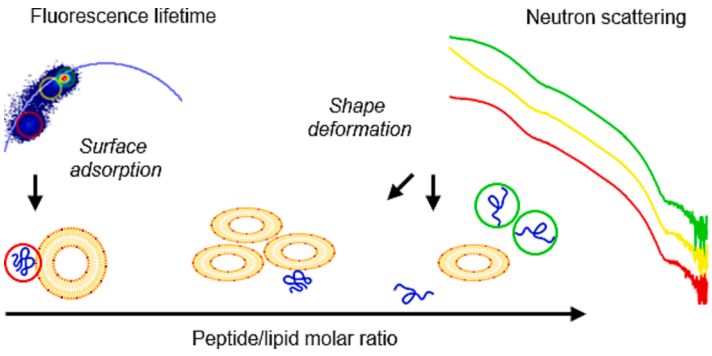

ARTICLE INFO

Keywords:
Cell-penetrating peptide
Mechanism
Membrane interaction
Small-angle neutron scattering
Fluorescence lifetime imaging microscopy

ABSTRACT

The cell-penetrating peptide penetratin and its analogues shuffle and penetramax have been used as carrier peptides for oral delivery of therapeutic peptides such as insulin. Their mechanism of action for this purpose is not fully understood but is believed to depend on the interactions of the peptide with the cell membrane. In the present study, peptide-liposome interactions were investigated using advanced biophysical techniques including small-angle neutron scattering and fluorescence lifetime imaging microscopy. Liposomes were used as a model system for the cell membrane. All the investigated carrier peptides induced liposome clustering at a specific peptide/lipid ratio. However, distinctively different types of membrane interactions were observed, as the liposome clustering was irreversible for penetratin, but fully or partly reversible for shuffle and penetramax, respectively. All three peptides were found to adsorb to the surface of the lipid bilayers, while only shuffle and penetramax led to shape deformation of the liposomes. Importantly, the peptide interactions did not disrupt the liposomes under any of the investigated conditions, which is advantageous for their application in drug delivery. This detailed insight on peptide-membrane interactions is important for understanding the mechanism of peptide-based excipients and the influence of peptide sequence modifications.

* Corresponding author.
E-mail addresses: ragna.diedrichsen@sund.ku.dk (R.G. Diedrichsen), valeria.vetri@unipa.it (V. Vetri), prevost@ill.fr (S. Prévost), vito.fodera@sund.ku.dk (V. Foderà), hanne.morck@sund.ku.dk (H.M. Nielsen).

https://doi.org/10.1016/j.jcis.2023.07.078
Received 6 February 2023; Received in revised form 27 June 2023; Accepted 12 July 2023
Available online 17 July 2023

1. Introduction

The low bioavailability of therapeutic peptides including insulin upon oral administration can be enhanced by employing cell-penetrating peptides (CPPs) as permeability enhancing excipients. The cationic CPP penetratin was previously shown to enhance insulin bioavailability in rats following nasal administration [1] and more recently, two of its analogues were demonstrated to be superior as carriers for insulin delivery from the intestine [2]. In those studies, insulin was co-administered in a physical mixture with the peptide excipients as carriers for enhancing insulin permeation across the intestinal epithelium. The resulting carrier peptide-mediated insulin delivery is proposed to be facilitated first by electrostatic interactions between the positively charged carrier peptides and the cell membrane with its negatively charged phospholipid head groups and glycosaminoglycans embedded into the lipid bilayer [3,4]. Following the initial electrostatic interactions, hydrophobic interactions between the phospholipid tails and the hydrophobic moieties in the amphiphilic peptides facilitate further interaction with and/or penetration of the carrier peptide into the cell membrane [4]. Thus, both the presence of cationic as well as nonpolar moieties in the peptide excipient are important for its membrane interaction.

Penetratin is a widely studied CPP and progress have been made in elucidating its mechanism of penetration into cells, which is generally accepted to involve direct translocation and endocytosis [5,6]. The amphiphilic peptide adopts an α-helical structure in the presence of sodium dodecyl sulfate (SDS) micelles as membrane models [7,8]. The analogues, shuffle and penetramax, consist of exactly the same 16 amino acids, thus represent the same molecular weight and the same number of cationic and hydrophobic moieties, which are both important for membrane interactions of CPPs [9]. Yet, in both peptides with shuffled sequences compared to penetratin, the alterations lead to different organization of hydrophobic clusters when coiled in α-helical structures as seen from the helical wheel representations (Fig. 1). The shuffled sequences have different groupings of uncharged amino acids resulting in a different hydrophobic moment as calculated using the HeliQuest calculator [10]. This might result in altered peptide folding upon interaction with membranes and might thus explain their reported superiority as carriers for insulin delivery efficiency relative to penetratin [2]. However, also the switch of the terminal cationic amino acids lysine (K) and arginine (R) in the amino acid sequence of penetramax compared to that of shuffle could induce subtle changes relevant for the function of the peptide [2,11].

To understand the impact of the amino acid position on the carrier peptide membrane interactions, the influence of carrier peptide type and concentration on interactions with liposomes was investigated using orthogonal scattering- and fluorescence-based techniques. Specifically, we aimed to provide mechanistic insights into the effect of reorganized peptide structure with regards to the effect of the different groupings of hydrophobic amino acids and switching the terminal cationic amino acids by investigating penetratin and its analogues, i.e., shuffle and penetramax. Such detailed information about the interactions at molecular level and physical changes in liposome size and shape will indeed allow deciphering structure-specific advantages of peptide excipients and close the knowledge gap in regards to their improved delivery effects.

2. Materials and methods

2.1. Materials

Human recombinant insulin (molecular weight (Mw): 5808 g/mol, activity: > 27.5 U/mg, and zinc content: < 1%) was manufactured by Sigma-Aldrich Fine Chemicals and purchased via Merck (Darmstadt, Germany). Non-labelled and *N*-terminally carboxyfluorescein (CF)-labelled L-form and non-labelled D-form of penetratin (RQIKIWFQNRRMKWKK), shuffle (RWFKIQMQIRRWKNKK), and penetramax (KWFKIQMQIRRWKNKR) (Mw (non-labelled/labelled): 3159/3404 g/mol including 7 trifluoroacetic acid (TFA) and purity: > 95%) were synthesized by Synpeptide (Shanghai, China). The 2-morpholin-4-ylethane sulfonic acid (MES, purity: > 99.5%) was obtained from PanReac AppliChem (Darmstadt, Germany). The [(2R)-3-hexadecanoyloxy-2-[(Z)-octadec-9-enoyl]oxypropyl] 2-(trimethylazaniumyl)ethyl phosphate (POPC) and [(2R)-1-[2,3-dihydroxypropoxy(hydroxy) phosphoryl]oxy-3-hexadecanoyloxypropan-2-yl] (Z)-octadec-9-enoate (sodium salt) (POPG) (purity: > 99%) were manufactured by Avanti Polar Lipids (Alabaster, AL, USA). The 1-[6-(dimethylamino)naphthalen-2-yl]dodecan-1-one (Laurdan, purity: > 97.0%) and dimethyl sulfoxide (DMSO, purity: > 99.9%) were purchased from Merck.

2.2. Sample preparation

10 mM MES in ultrapure water adjusted to pH 6.5 (MES buffer) was used in all experiments except for small-angle neutron scattering (SANS) in which 10 mM MES in deuterated water (D_2O) adjusted to pH 6.5 (MES-D_2O) was used. Insulin was dissolved at 9 mg/mL in ultrapure water purified by a PURELAB flex (ELGA, High Wycombe, UK) upon addition of hydrochloric acid (HCl) to a final concentration of 10 mM HCl. The carrier peptides were dissolved at 4–8 mg/mL in MES buffer in polypropylene tubes (Scientific Specialties, Lodi, CA, USA). The samples

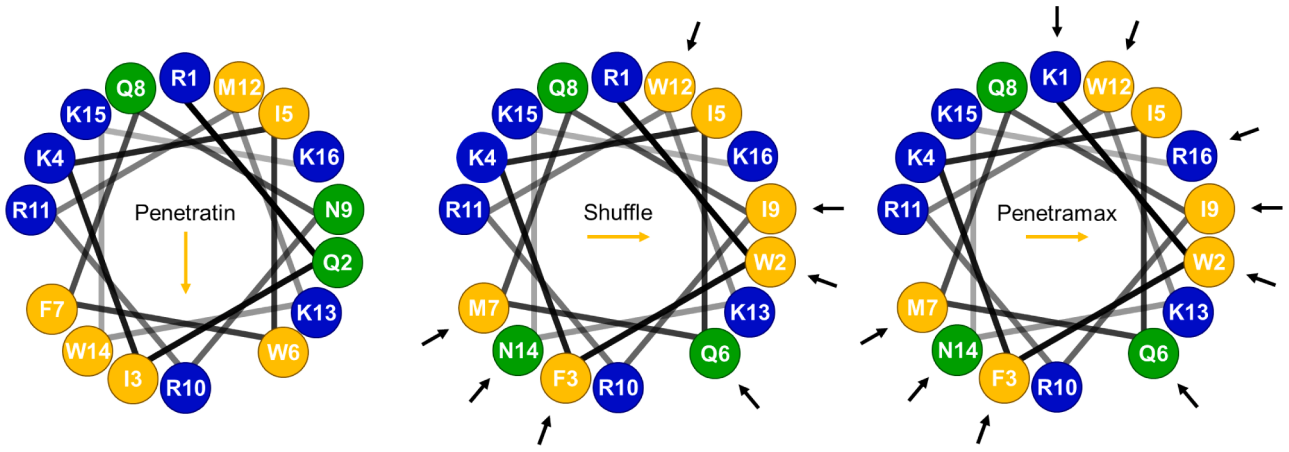

Fig. 1. Peptide sequences of the amphiphilic penetratin and its analogues shuffle and penetramax displayed as helical wheel projections. Nonpolar (yellow), polar uncharged (green), and polar positively charged (blue) amino acids. Shuffled amino acids in comparison to penetratin are marked with black arrows. The yellow arrows represent the hydrophobic moment.

were filtered through 0.2 μm cellulose acetate filters (Toyo Roshi Kaisha, Tokyo, Japan) and the content of insulin and carrier peptide was quantified in the filtrate by absorbance at 280 nm using a Nanodrop 2000c (Thermo Fisher Scientific, Waltham, MA, USA) using theoretical extinction coefficients of 6710 and 11000 M^{-1} cm^{-1} for insulin and the carrier peptides, respectively [12]. The stock samples were stored at −80 °C for up to 2 weeks until use.

2.3. Liposome preparation

Large unilamellar vesicles containing 80:20% (mol/mol) POPC:POPG lipids were prepared by extrusion. POPC and POPG lipids in chloroform were mixed in round bottom flasks and vortexed thoroughly. The chloroform was evaporated under rotatory evaporation overnight. The lipid film was hydrated to 20 mg/mL lipids in MES buffer for all experiments, except for the dynamic light scattering (DLS) and absorbance measurements in which 30 mg/mL lipid concentration was used, with thorough vortexing every 10 min for 1 h. The resulting vesicle dispersion was left to rest for 1 h. The larger multilamellar vesicles were disrupted by prefiltering through polycarbonate membranes with 200 nm pore size (Whatman, Florham Park, NJ, USA) three times and sized by extrusion through 100 nm membranes (Avanti Polar Lipids) 21 times using a mini-extruder (Avanti Polar Lipids). The lipid content in the liposome dispersion was quantified using a phospholipid assay kit (MTI Diagnostics, Idstein, Germany) as described by the manufacturer. Standard samples were prepared from non-extruded liposomes. With this kit, the lipid concentration was confirmed to be in the range of 0.83–1.08 relative to the theoretical concentration. For reasons of simplicity, the theoretical molar peptide-to-lipid ratios are used throughout the manuscript. The liposomes were stored at 4 °C for up to 2 weeks until use.

2.4. Dynamic light scattering (DLS)

Size distribution of carrier peptide-liposome samples alone and in presence of insulin was investigated by DLS using a Zetasizer Nano ZSP (Malvern Panalytical, Malvern, UK). A volume of 100 μL samples of 10 mg/mL liposomes consisting of 80:20% (mol/mol) POPC:POPG lipids in the presence of 0.18–1.41 mg/mL L- and D-forms of penetratin, shuffle, and penetramax (0.006–0.048 peptide/lipid) alone or in mixture with 0.11–0.34 mg/mL insulin (0.25 insulin/peptide) in MES buffer was measured in ultraviolet (UV) micro cuvettes (Brand, Wertheim, Germany) at a 173° angle with 11 runs of 10 s/run in 3 measurements.

2.5. UV–visible absorbance spectroscopy

Turbidity of carrier peptide-liposome samples alone and in presence of insulin was measured as absorbance using the Nanodrop 2000c (Thermo Fisher Scientific). A volume of 2 μL samples of 10 mg/mL liposomes consisting of 80:20% (mol/mol) POPC:POPG lipids in the presence of 0.18–1.41 mg/mL L- and D-forms of penetratin, shuffle, and penetramax (0.006–0.048 peptide/lipid) alone or in mixture with 0.11–0.34 mg/mL insulin (0.25 insulin/peptide) in MES buffer was measured at 600 nm on the pedestal of 4–5 drops.

2.6. Electrophoretic light scattering (ELS)

Zeta potential of carrier peptide-liposome samples was investigated by ELS using the Zetasizer Nano ZSP (Malvern Panalytical). A volume of 700 μL samples of 10 mg/mL liposomes consisting of 80:20% (mol/mol) POPC:POPG lipids in the presence of 0.18–1.24 mg/mL L-penetratin, L-shuffle, and L-penetramax (0.006–0.042 peptide/lipid) in MES buffer was measured in folded capillary cells (Malvern Panalytical) with 22 runs in 3 measurements.

2.7. Small-angle neutron scattering (SANS)

Scattering intensity of carrier peptide-liposome samples was investigated by SANS using the D11 instrument at the Institut Laue-Langevin (ILL, Grenoble, France). For sample preparation, peptides were quantified using a Nanodrop One (Thermo Fisher Scientific). A volume of 300 μL samples of 10 mg/mL liposomes consisting of 80:20% (mol/mol) POPC:POPG lipids in the presence of 0.18–1.24 mg/mL penetratin, shuffle, and penetramax (0.006–0.042 peptide/lipid) in MES-D_2O was measured in 1 mm Hellma quartz cuvettes (Hellma, Müllheim, Germany) at detector distances of 1.4 m, 8 m, and 39 m, resulting in a q range of 0.001–0.5 $Å^{-1}$. A 2 mm cuvette was used for measurement of peptides in the absence of liposomes.

Data were analyzed using SasView [13]. The liposomes without peptides were fitted to a sphere model with core shell structure [14] with a log-normally distributed core radius (R_c) and a normally distributed homogeneous lipid bilayer thickness (t) according to the equation:

$$P(q) = \int LogNormal(R_c, s) \int Normal(t, \sigma) F^2(q, R_c, t) dt dR_c$$

$$F(q, R_c, t) = 3\frac{f(q, R_c + t) - f(q, R_c)}{\left[(R_c + t)^3 - R_c^3\right]}$$

$$f(q, R) = \frac{\sin qR_c - qR_c \cos qR_c}{q^3}$$

The fit was refined at low q to account for excluded volume with a hard sphere structure factor using the “decoupling approximation” [14]:

$$S^{eff}(q) = 1 + \frac{\langle F(q)\rangle^2}{\langle F^2(q)\rangle}(S(q) - 1)$$

where the brackets denote the average size distribution of the overall liposome radius and S(q) is the hard sphere structure factor. The scattering length density (SLD) of liposomes was calculated using a SLD calculator provided by NIST Center for Neutron Research [15] with densities of 1.015 g/cm^3 for the POPC lipids [16] and 1.067 g/cm^3 for the POPG lipids [17] and assuming deuterium exchange with the two labile protons of the POPC lipids.

2.8. Cryogenic transmission electron microscopy (cryo-TEM)

Carrier peptide-liposome samples were imaged by cryo-TEM at the Core Facility for Integrated Microscopy (CFIM, Copenhagen, Denmark). A volume of 3 μL samples of 10 mg/mL liposomes consisting of 80:20% (mol/mol) POPC:POPG lipids in the presence of 0.35–1.24 mg/mL penetratin, shuffle, and penetramax (0.012–0.042 peptide/lipid) in MES buffer was added to hydrophilized lacey carbon films on 300 mesh copper grids (Ted Pella, Redding, CA, USA) at room temperature and 100% humidity using a Vitrobot Mark IV (FEI, Eindhoven, Netherland). The grids were blotted for 3 s with a blot force of 0 to remove excess sample and plunged into liquid nitrogen-cooled ethane. The samples were imaged at a voltage of 200 kV under a low-dose rate using a Tecnai G2 20 TWIN (FEI) equipped with a High-Sensitive (HS) 4 k × 4 k Eagle camera (FEI) with image acquisition at a magnification of 5000× or 29,000×. The images were processed using ImageJ (National Institutes of Health, Bethesda, MD, USA).

2.9. Two-photon excitation, confocal, and fluorescence lifetime imaging microscopy (FLIM)

Carrier peptide-liposome samples were imaged using a Leica TCS SP5 confocal scanning microscope equipped with a 63×/1.4NA oil objective (Leica Microsystems, Wetzlar, Germany). For sample preparation, peptides were quantified using a V-770 UV–Visible/NIR spectrophotometer

equipped with a SAH-769 One Drop accessory (JASCO Europe, Cremella, Italy). The liposomes were stained 1:1000 (mol/mol) with Laurdan dissolved in DMSO for 5 h prior use. The carrier peptides contained 1% (mol/mol) CF-labelled peptide. A volume of 200 μL samples of 10 mg/mL liposomes consisting of 80:20% (mol/mol) POPC:POPG lipids alone or in the presence of 0.18–1.24 mg/mL penetratin, shuffle, and penetramax in MES buffer was imaged in Nunc Lab-Tek II chambered coverglass (Thermo Fisher Scientific). Images were acquired in 1024 × 1024 pixels and at a scanning speed of 200 Hz. Laurdan fluorescence was analysed with two-photon excitation at 780 nm using a Mai Tai Ti: Sapphire Ultrafast NIR Laser (Spectra-physics, Milpitas, CA, USA) and emission was collected in the range of 430–460 nm. CF fluorescence was analysed with excitation at 493 nm using the white light laser (Leica Microsystems) and emission was collected in the range of 515–600 nm with a pinhole corresponding to 1 airy unit. Images were processed and quantified using Leica LAS X software (Leica Microsystems).

Lifetime of Laurdan-stained liposomes or CF-labelled peptides was investigated by FLIM. Images were acquired in 256 × 256 pixels with emission in the range of 430–470 nm for analysis of Laurdan fluorescence or emission in the range of 510–620 nm for analysis of CF fluorescence. Data were analysed by the phasor approach [18] with calibration using fluorescein with a lifetime of 4.0 ns [19,20] using SimFCS software (Laboratory for Fluorescence Dynamics, Irvine, CA, USA). The phasor approach is a fit free analysis that maps each pixel of the image to a point in the phasor plot according to the measured fluorescence lifetime. Single exponential lifetimes are distributed on a universal circle from coordinate (0,0) to coordinate (1,0). Longer lifetimes are mapped on the universal circle toward coordinate (0,0), while shorter lifetimes are mapped toward coordinate (1,0). Complex, multi-exponential decays are distributed inside the universal circle [18]. By selecting a lifetime distribution using a blue cursor, pixels are colour-coded in the lifetime maps accordingly.

2.10. UV–Visible fluorescence spectroscopy

Fluorescence of CF-labelled peptides in the presence of liposomes was measured using a FP-8500 spectrofluorometer (JASCO Europe). A volume of 800 μL samples of 0.18–1.24 mg/mL penetratin, shuffle, and penetramax containing 1% (mol/mol) CF-labelled peptide alone or in the presence of 10 mg/mL liposomes consisting of 80:20% (mol/mol) POPC:POPG lipids in MES buffer was measured in Brand semi-micro cuvettes (BrandTech, Essex, CT, USA) with excitation at 475 nm and emission in the range of 475–650 nm in three measurements. Data were background corrected using buffer or liposomes alone for samples containing peptides alone or peptides in the presence of liposomes, respectively, and scaled to peak maximum.

The selected fluorophore was verified not to influence the carrier peptide-liposome interactions with similar size distribution when using 1% (mol/mol) of CF-labelled peptides as compared to only non-labelled peptides (Fig. S1).

2.11. Circular dichroism (CD)

Secondary structure of carrier peptides in the presence of liposomes was investigated by CD using a Chirascan CD spectrometer (Applied - Photophysics, Leatherhead, UK). A volume of 40 μL samples of 0.18–1.24 mg/mL penetratin, shuffle, and penetramax in the presence of 10 mg/mL liposomes consisting of 80:20% (mol/mol) POPC:POPG lipids in MES buffer was measured in a demountable 0.1 mm Spectrosil quartz cuvette (Starna Scientific, Pfungstadt, Germany) at 190–280 nm in five scans. Data were background corrected using buffer or liposomes alone, subtracted the baseline at 280 nm and converted to mean residue ellipticity (MRE) by the equation:

$$MRE = (\theta \times 100)/(l \times C \times N)$$

where θ is the ellipticity, l is the path length, C is the concentration, and N is the number of residues. The relative content of specific structures was estimated by the algorithm beta structure selection (BeStSel), developed by Micsonai *et al.* for fold recognition and secondary structure determination [21].

3. Results and discussion

Carrier peptide interactions with membranes were evaluated as a function of size and shape of liposomes, as cell membrane mimics, in the presence of the different peptides by using scattering techniques. The degree of interaction, specifically whether the peptides were located on the surface of the liposomes or inside the lipid bilayers, was further investigated using fluorescence techniques. The liposome lipid concentration was kept constant at 10 mg/mL (13 mM), while increasing the peptide concentration in the range 0.18–1.41 mg/mL (79–630 μM) and hereby the peptide/lipid ratio (0.006–0.048 peptide/lipid molar ratio).

3.1. Size and charge of liposome samples change in the presence of carrier peptides

Size distributions of liposomes and the effect of increasing carrier peptide-to-lipid ratios were first investigated by DLS and absorbance measurements (Fig. 2A-C). The liposomes alone and in the presence of 0.18–0.27 mg/mL L-peptide (0.006–0.009 peptide/lipid) displayed a size of 103–105 nm when expressed as Z-average (Fig. 2A). The samples were monodisperse with a polydispersity index (PDI) of 0.1 (Fig. 2B). Liposomes in presence of 0.35 mg/mL L-peptide (0.012 peptide/lipid) showed larger sizes with mean values above 1 μm and a high turbidity of 0.8–0.9 at 600 nm (Fig. 2C). The liposome mean size reverted concentration dependently in the presence of 0.44–1.41 mg/mL L-shuffle and L-penetramax (0.015–0.048 peptide/lipid) to a size of 130–136 nm at 1.41 mg/mL peptide (0.048 peptide/lipid). In contrast, the size distributions of liposomes in the presence of 0.88–1.41 mg/mL L-penetratin (0.030–0.048 peptide/lipid) remained high and were accompanied by a PDI of 1. In general, the larger size samples were highly polydisperse with PDIs of or>0.4.

The zeta potential of liposomes and the effect of increasing amounts of carrier peptides were investigated by ELS measurements (Fig. 2D). The carrier peptides alone in a concentration of 1.24 mg/mL had zeta potentials of +13.9 ± 2.7 mV, +47.9 ± 2.3 mV, and +32.9 ± 1.4 mV for penetratin, shuffle, and penetramax, respectively, while the liposomes alone had a zeta potential of −56.7 ± 1.4 mV. The zeta potential of the carrier peptide-liposome mixture increased as a function of carrier peptide concentration and reached plateau at +11.1 ± 1.9 mV, +16.6 ± 0.7 mV, and +17.2 ± 0.9 mV in presence of 1.24 mg/mL (0.042 peptide/lipid) penetratin, shuffle, and penetramax, respectively, reflecting that a close to neutral net charge correlated with larger structures and polydisperse samples.

Interactions of cationic peptides with cell membranes may indeed lead to effects on e.g., the cellular metabolic activity, which has been shown to be influenced by the stereochemistry of the carrier peptides as well as presence of a co-administered therapeutic cargo peptide [2,22]. Here, we demonstrate that the actual carrier-peptide-liposome interactions were similar for the L-and D-forms of the carrier peptides both alone and in presence of insulin (Fig. S2), and thus seemed independent of stereochemistry and presence of a net negative cargo. Subsequent studies on carrier peptide-liposome interactions were therefore performed only with the L-peptides.

3.2. Carrier peptides induce reversible liposome clustering

At physiological pH including the pH 6.5 used in the present study, the cationic peptides will be positively charged, while the anionic phosphatidylglycerol (PG) lipid head group in the liposomes will be negatively charged favouring electrostatic interactions. At low molar ratios of 0.006–0.009 peptide/lipid, the size distribution of liposomes

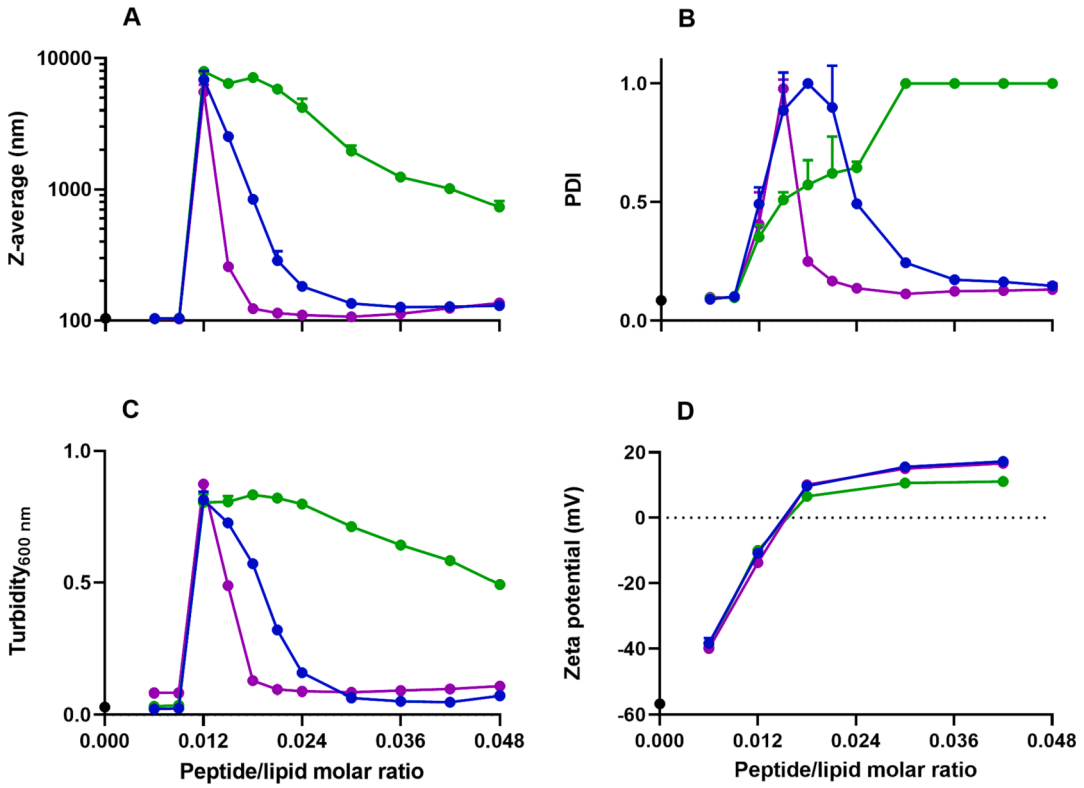

Fig. 2. Size distribution expressed as Z-average (A), PDI (B), turbidity at 600 nm (C), and zeta potential (D) of 10 mg/mL liposomes consisting of 80:20% (mol/mol) POPC:POPG lipids alone (black, at coordinate (0,y)) or in presence of 0.18–1.41 mg/mL L-penetratin (green), L-shuffle (purple), and L-penetramax (blue) (0.006–0.048 peptide/lipid) in MES buffer investigated by DLS, turbidity, and ELS measurements. Mean ± standard deviation (SD) (n = 3 for DLS and ELS, n = 4–5 for turbidity, where n is the number of repeated measurements).

was similar to that of the liposomes alone with an overall negative charge of the samples, keeping the colloidal system stabilized by repulsive forces (Fig. 2A,D). At the molar ratio of 0.012 peptide/lipid, the large sizes indicate clustering of the liposome. This is likely due to the overall charge approaching zero, which favours attractive forces and, in turn, causes clustering. Liposome clustering was previously demonstrated for penetratin [23–25], but has not been investigated for shuffle and penetramax. Specifically, a study by Persson *et al.* showed clustering of liposomes consisting only of anionic 3-[2,3-dihydroxypropoxy(hydroxy)phosphoryl]oxy-2-[(Z)-octadec-9-enoyl]oxypropyl] (Z)-octadec-9-enoate (DOPG) lipids in the presence of penetratin (0.074 peptide/DOPG lipid) [23]. This reported value is similar to that observed in the present study using liposomes consisting of 80:20% (mol/mol) POPC:POPG lipids as the 0.012 peptide/lipid molar ratio corresponds to 0.060 peptide/POPG lipid. Persson *et al.* found the liposome clustering to be time-dependent with reversal after 1.5 h, while constant at a higher peptide concentration (0.133 peptide/DOPG lipid) [23]. In contrast, the present study showed that with penetratin the liposome clustering was observed not to depend on time at the investigated concentrations. However, the liposome clustering did revert in presence of larger amounts of shuffle and penetramax (0.018–0.042 peptide/lipid) (Fig. 2A). Penetratin is known to translocate across biological membranes [26], consequently decreasing the amount of peptide bound to the outer leaflet of the lipid bilayers. This could explain the reverted liposome clustering when in presence of larger amounts of shuffle and penetramax as peptide translocation across the lipid bilayer would lead to a smaller amount of peptide at the liposome surface and, consequently, to a reversal of the liposome clustering. However, penetratin has also been shown to interact with liposomes consisting of 95:5% (mol/mol) POPC:POPG lipids with no translocation through the lipid bilayer [27]. This might be a more likely explanation for the observations in the present study, where a homogenous peptide distribution on the liposome surface leads to a more stable configuration of the single liposomes due to repulsive forces between surface-coated individual liposomes. The fact that the zeta potential of the peptide coated colloids are more positive in the case of penetramax and shuffle compared to that of penetratin support this explanation and is in accordance with the positive zeta potential of the overall system comprising peptide-covered liposomes and peptides freely in solution (Fig. 2D).

3.3. Size and shape of liposomes change in the presence of carrier peptides

Scattering intensity of liposomes and the effect of increasing concentrations of carrier peptides were investigated by SANS (Fig. 3A) [28]. The scattering intensity (I) of the liposomes is plotted as a function of the scattering vector (q) in Fig. S3A. The value of q depends on the angle at which neutrons scattered by the sample molecules are detected with large structures detected at low q. For liposomes without peptide, five observations were made as marked in the figure. 1) At high q, a form factor oscillation corresponding to the lipid bilayer thickness (t) of 36.5 Å ($t = 2\pi / q$). Only one form factor oscillation is present, suggesting unilamellar liposomes. 2) At mid q in the Kratky region ($0.025\ Å^{-1} < q < 0.05\ Å^{-1}$), a slope with a power law of q^{-2} is seen and is characteristic for flat structures such as lipid bilayers. 3) At the lowest q in the Guinier region ($q < 0.0025\ Å^{-1}$), the intensity reached a plateau corresponding to a Radius of gyration (R_g) of 423 Å. The intensity of forward scattering (I(0)) was proportional to a Porod volume (V_p) of $6 \times 10^7\ Å^3$. Based on the Porod volume and the lipid bilayer thickness, the outer radius was calculated to be 362 Å. 4) At low q between the Guinier and Kratky regions, a smeared form factor oscillation was evident corresponding to a liposome diameter (D) of 850 Å ($D = 2\pi / q$). This was consistent with the radius determined by Guinier approximation and larger than the radius calculated based on the Porod volume, but acceptable

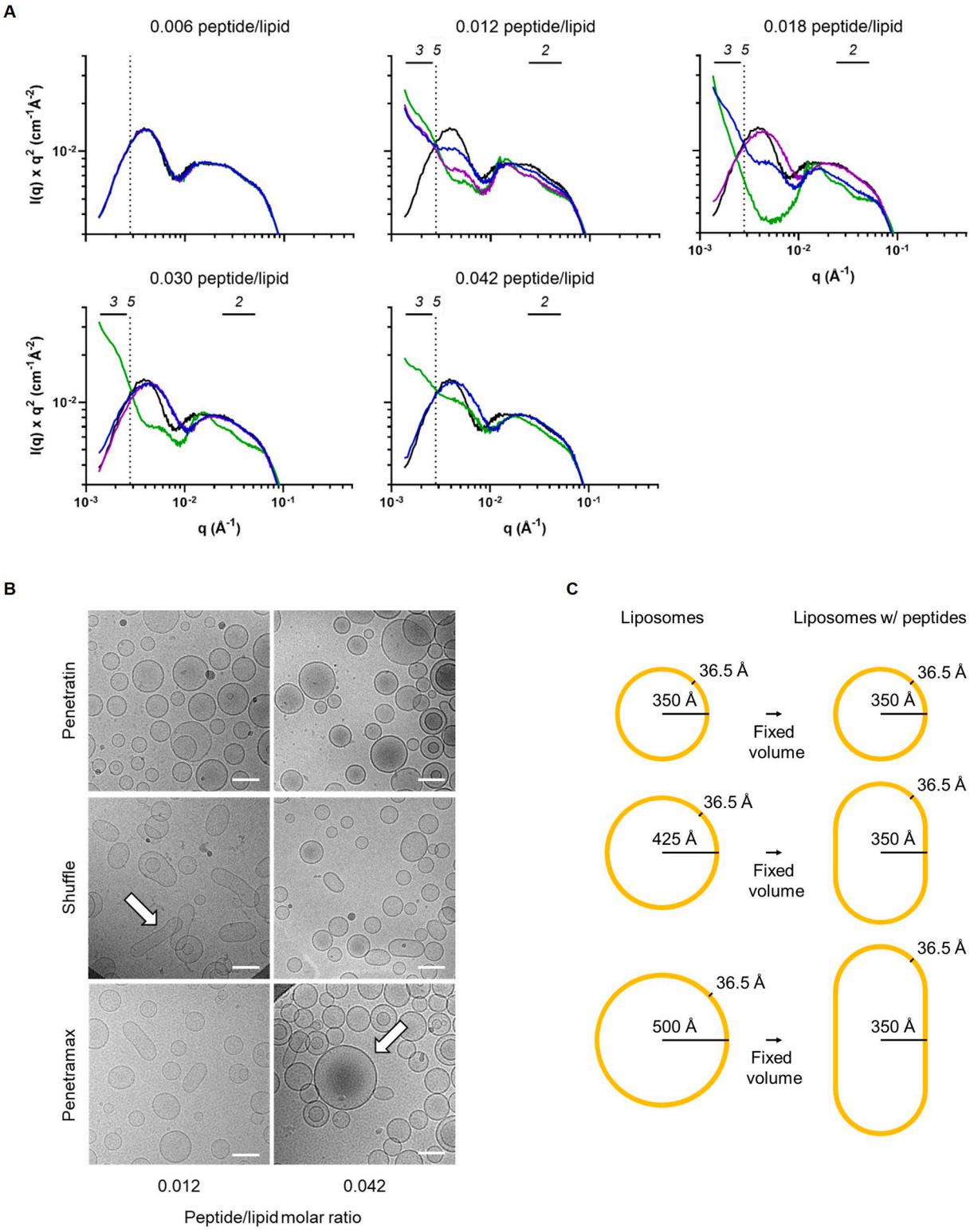

Fig. 3. (A) Scattering intensity of 10 mg/mL liposomes consisting of 80:20% (mol/mol) POPC:POPG lipids alone (black) or in the presence of 0.18, 0.35, 0.53, 0.88, and 1.24 mg/mL penetratin (green), shuffle (purple), and penetramax (blue) (0.006–0.042 peptide/lipid) in MES-D_2O investigated by SANS. Experimental data are presented with statistical SD. (B) Representative images of 10 mg/mL liposomes consisting of 80:20% (mol/mol) POPC:POPG lipids in the presence of 0.35 and 1.24 mg/mL penetratin, shuffle, and penetramax (0.012–0.42 peptide/lipid) in MES buffer investigated by cryo-TEM (n > 10, where n is the number of images). Scale bar: 100 nm. Examples of ellipsoidal and fused liposomes are marked with arrows. (C) Illustration of proposed theory.

considering the polydispersity of the sample. 5) The liposomes displayed a bell-shaped peak in the Kratky plot (Fig. S3B), characteristic for spherical structures. The liposome profiles were fitted to a sphere model with core shell structure accounting for interparticle interactions in terms of excluded volume (Fig. S3; grey curve). The fit could be refined further to account for electrostatic repulsion between the negatively charged PG head groups, but the repulsion seemed sufficiently screened by the MES buffer and therefore disregarded in the fit. The SLD profile of

the lipid bilayer could be refined by distinction of the hydrated head groups (SLD = 2.13 × 10^6 Å^{-2} in an 80:20% (mol/mol) mixture) and of the acyl chains (SLD = -0.29 × 10^6 Å^{-2}). The dehydrated acyl chains thus have a higher contrast to the solvent (SLD = 6.38 × 10^6 Å^{-2} for D_2O). The effect of the refined SLD profile was, however, negligible in the fit and therefore disregarded for reasons of simplicity.

For liposomes with increasing amounts of peptide, five observations were made (Fig. 3A, Fig. S4). 1) The high and mid q ranges are negligibly affected by the presence of peptides, indicative of unchanged lipid bilayer thickness and liposome amount (Fig. S4). Similarly, the antimicrobial peptide indolicidin has been shown not to affect the lipid bilayer thickness [29]. 2) When displayed in the Kratky plot, however, a shift of the scattering intensity is observed (Fig. 3A). This is suggestive of lamellar stacking such as multilamellar vesicles or, alternatively, clustered liposomes with adjacent shells. The CPP nonaarginine has previously been demonstrated to induce vesicle multilamellarity [30]. However, with only one form factor oscillation at high q, this is not considered as the main explanation for the observations in the SANS profiles. 3) At the lowest q (q < 0.0025 Å^{-1}), a distinct increase is detected in the scattering intensity with a power law > -2.4 at a peptide concentration of 0.35 mg/mL (0.012 peptide/lipid). This indicates formation of dense structures > 0.5 μm detectable in the investigated q range, confirming the liposome clustering also observed by the DLS analysis (Fig. 2A). The increase in scattering intensity, and thus the liposome clustering, reverted at higher peptide concentrations, specifically at concentrations of and higher than 0.53 mg/mL shuffle (0.018 peptide/lipid) and 0.88 mg/mL penetramax (0.030 peptide/lipid), but not in the case of penetratin (Fig. 3A, Fig. S4). Alternatively, the distinct increase could be a result of vesicle fusion as also demonstrated for nonaarginine [30]. However, liposome fusion is unlikely to revert and is therefore not considered as the main explanation for the increase. 4) At low q, the form factor oscillation corresponding to the liposome diameter was changed with decreased intensity and slightly shifted position of the oscillation (Fig. S4). The effects partly reverted at concentrations of 0.53 mg/mL shuffle (0.018 peptide/lipid) and of 0.88 mg/mL penetramax (0.030 peptide/lipid), but not in the case of penetratin. This is in direct correlation with the distinctly increased scattering intensity (3rd observation). 5) The SANS profiles exhibit an isosbestic point, i.e., all curves cross at a particular q-value (q ≈ 0.0028 Å^{-1} corresponding to 2244 Å; marked with dashed line), with the exception of liposomes with 0.53 mg/mL penetratin (0.018 peptide/lipid) (Fig. 3A, Fig. S4). Scattering intensity of the peptides alone is provided in the Supplementary material (Fig. S5).

To support the interpretation of the SANS data, liposomes alone and in the presence of peptides were imaged using cryo-TEM (Fig. 3B). The liposomes alone mainly displayed a spherical shape (Fig. S6). When in presence of shuffle and penetramax, the liposomes displayed both spherical and elongated shapes, while the liposomes mainly displayed a spherical shape in the presence of penetratin (Fig. 3B). Evidence of some fused liposomes in the size range of 0.2–1 μm was observed with all three peptides. Representative overview images are included in Fig. S7.

3.4. Carrier peptides deform the shape of liposomes

The 5th observation of an isosbestic point can be explained by clustering of spheres (Fig. 3A). However, to fully explain clustering, two isosbestic points should be present at a q-ratio of 2 for $q_1 = \pi / D$ and $q_2 = 2\pi / D$, where D is the distance between the centers of mass, as demonstrated in simulated SANS profiles (Fig. S8). With a distance of 2244 Å, q_1 would correlate to 0.0014 Å, where no isosbestic point was observed in the SANS profiles (Fig. 3A). An alternative explanation of the isosbestic point can be a change of proportions between two populations as also demonstrated in other systems [31]: one population of liposomes unaffected by the peptides and another population of liposomes affected by the peptides. To probe the population of peptide-affected liposomes, the SANS profiles of the liposomes in mixture with peptides were subtracted a fraction (c) of the liposomes alone (Fig. S9), resulting in the calculated SANS profiles displayed in Fig. S10. For example, at 0.18 mg/mL peptide (0.006 peptide/lipid), 90% of the scattering intensity corresponded to unaffected liposomes, while the remaining 10% represents the other population. The calculated data are comparable to that observed in the original SANS profiles, but the form factor oscillation is shifted toward higher q indicating a smaller size distribution. Specifically, the shift was from 0.010 Å for liposomes alone to 0.012–0.015 Å for the calculated data (Fig. S10; the dotted lines mark the approximate plateau of the form factor oscillations). Three explanations for this shift can be made. 1) Only small liposomes are affected by the peptides, meaning that the peptide-liposome interactions are dependent on surface tension with a higher surface tension of the smaller liposomes. However, this is not supported by the observations made using cryo-TEM (Fig. 3B). 2) The liposomes are becoming smaller as a result of lipid exchange. This is, however, unlikely to be reversible as was the case for liposomes with shuffle and penetramax. 3) The peptides influence the curvature of the liposomes, resulting in elongation and thus a smaller cross-section with no lipid exchange, i.e., unaffected volume distribution, as illustrated in Fig. 3C. The form factor oscillation remains shifted and thus liposome elongation remains present upon reverted liposome clustering. This explanation is supported by cryo-TEM observations (Fig. 3B). Indeed, CPPs are known to induce membrane curvature prior to or in the process of pore formation and endocytosis [32]. Additionally, the spatial orientation of *trans*-membrane segments of proteins has been proposed to induce membrane curvature [33]. In our study, and specifically in the case of penetratin, mainly spherical liposomes were observed. The shift might thus be explained by lamellar stacking of adjacent liposomes with the non-reversible liposome clustering rather than induced liposome elongation (Fig. S10). As mentioned previously, the hydrophobic interactions might be important for the action of the carrier peptides considering their different groupings of hydrophobic amino acids displayed in helical wheel projections of the shuffled peptide sequences. This might thus explain the different types of liposome interactions with penetratin compared to shuffle and penetramax. We have previously investigated the carrier peptide-liposome interactions using isothermal titration calorimetry [2]. Interestingly, the study revealed no significant difference in binding affinity, while shuffle and penetramax did have higher binding capacities than penetratin. The reversible liposome clustering in the cases of shuffle and penetramax is thus likely a result of repulsion by the increased positive charge on the liposome surface supporting the DLVO (Derjaguin, Landau, Verway and Overbeek) theory describing the balance between attraction and repulsion between colloids. In addition to the higher binding capacity as well as the higher zeta potential of shuffle and penetramax compared to penetratin support this explanation. A higher amount of positively charged peptide bound to lipid bilayers such as the cell membrane might be favourable in relation to carrier peptide-mediated insulin delivery, considering that we have previously demonstrated that shuffle and penetramax are superior to penetratin as peptide excipients for enhancing transepithelial insulin permeation [2].

3.5. Carrier peptides and liposomes are co-localized in the clusters

Laurdan-stained liposomes (red) with increasing amounts of CF-labelled peptides (green) were imaged using fluorescence microscopy (Fig. 4A, Fig. S11). Image acquisition and processing were kept constant for all images, resulting in low fluorescence intensity at low peptide concentration. The intensity of penetratin alone was notably lower compared to that of shuffle and penetramax (Fig. S12). Homogeneous samples of both liposomes and peptides were observed at 0.18 mg/mL peptide (0.006 peptide/lipid) (Fig. 4A). At 0.35 mg/mL peptide (0.012 peptide/lipid), large structures (>1 μm) were observed for all peptides with co-localization of the liposomes and peptides, confirming the liposome clustering observed by the DLS and SANS investigations

(Fig. 2A, Fig. 3A). The liposome clustering was accompanied by a decrease in the fluorescence intensity in areas without clusters, i.e., representing freely diffusing peptides, when compared to 0.35 mg/mL peptide alone (Fig. S13), indicating that the peptides are primarily located in the clusters and thus associated with the liposomes. At high concentrations of peptide (0.88–1.24 mg/mL corresponding to 0.030–0.042 peptide/lipid), clustered liposomes were observed for penetratin, only freely dispersed liposomes were observed for shuffle, whereas a mixture of freely dispersed and clustered liposomes were observed for penetramax (Fig. 4A). The liposome clustering is thus observed to be only partly reversible in the case of penetramax under the used experimental conditions. The fluorescence intensity in areas without clusters were similar to that of 1.24 mg/mL peptide alone, indicating that the peptides were freely dissolved, i.e., excess peptide did not associate with the liposomes.

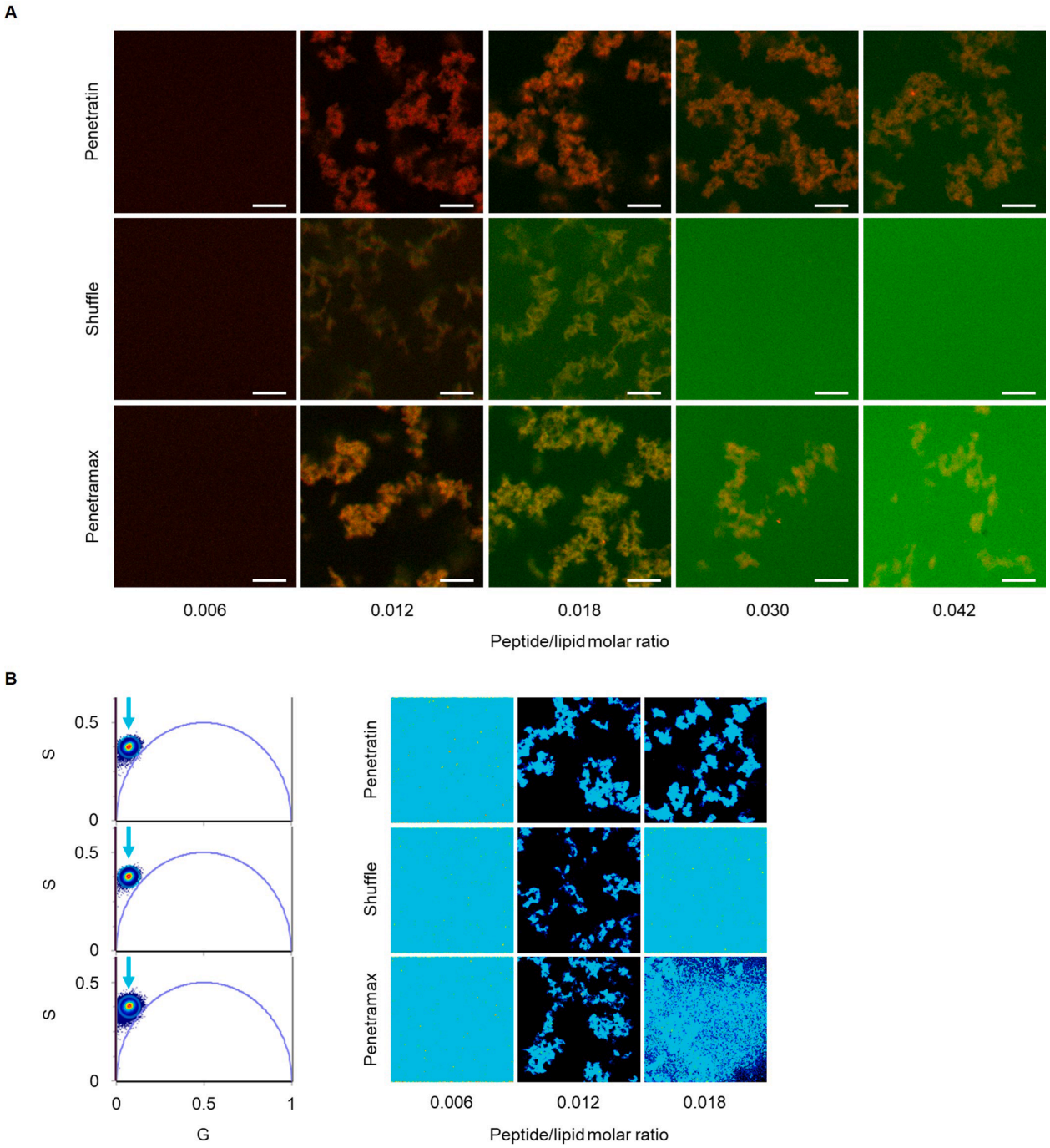

Fig. 4. (A) Representative merged images of 10 mg/mL Laurdan-stained liposomes consisting of 80:20% (mol/mol) POPC:POPG lipids (red) in the presence of 0.18, 0.35, 0.53, 0.88, and 1.24 mg/mL CF-labelled penetratin, shuffle, and penetramax (green) (0.006–0.042 peptide/lipid) in MES buffer investigated by fluorescence microscopy (n = 3, where n is the number of images). Scale bar: 5 μm. (B) Representative lifetime displayed in phasor plots, where G and S are phasor vectors (blue circle, left) and lifetime maps (right) of 10 mg/mL Laurdan-stained liposomes consisting of 80:20% (mol/mol) POPC:POPG lipids in the presence of 0.18–1.24 mg/mL penetratin (top), shuffle (middle), and penetramax (bottom) (0.006–0.042 peptide/lipid) in MES buffer investigated by FLIM (n = 3, where n is the number of repeated measurements). The lifetime maps are coloured according to the lifetime distribution selected by the blue circle in the phasor plot. The position of the lifetime distribution of Laurdan-stained liposomes alone are marked with blue arrows.

3.6. Environment in Laurdan-stained liposomes is unchanged in the presence of carrier peptides

Membrane fluidity of Laurdan-stained liposomes and the effect of carrier peptides were investigated by FLIM (Fig. 4B). Fluorescence intensity images of Laurdan-stained liposomes alone and in the presence of peptides are provided in the Supplementary material (Fig. S14A, Fig. S15). The fluorescence lifetime of the Laurdan dye is related to the polarity of the environment surrounding the dye, where water penetration into the membrane would typically change the membrane fluidity and hereby the Laurdan fluorescence lifetime [34,35]. In the generated phasor plots, the Laurdan fluorescence lifetime was superimposed both for liposomes alone and for liposomes in presence of the peptides (Fig. S14B,C, Fig. 4B). This indicates that the Laurdan dye environment and thus membrane polarity of the liposomes was not changed by the peptides. The lifetime distributions were located slightly outside the universal circle, as has previously been observed both in cellular [34] and synthetic membranes [36]. This was attributed to a highly heterogeneous environment surrounding the Laurdan dye.

3.7. Environment around CF-labelled carrier peptides is changed in the presence of liposomes

Fluorescence lifetime of CF-labelled peptides and the effect of liposomes was investigated by FLIM (Fig. 5A). Fluorescence intensity maps of CF-labelled peptides alone and in the presence of liposomes are provided in the Supplementary material (Fig. S16A, Fig. S17). For increasing concentrations of peptides in the presence of liposomes, three distributions of the CF fluorescence lifetime were distinguishable in the phasor plots (Fig. 5A). 1) At 0.18 mg/mL peptide (0.006 peptide/lipid), the CF fluorescence lifetime (red cursors) was complex and distributed towards longer lifetimes than that of freely diffusing peptide, i.e., in the absence of liposomes; the location of which is marked with green arrows and reported in Supplementary material (Fig. S16B). The longer CF fluorescence lifetime indicate a different environment surrounding the peptides, likely due to close association of the peptides with the liposomes and thus peptide-liposome interactions. For means of comparison, data on 0.18 mg/mL (0.006 peptide/lipid) CF-labelled penetratin, shuffle, and penetramax in the presence of liposomes are also displayed in Fig. S18. The lifetime distribution was shifted towards slightly shorter lifetimes for penetramax compared to that for penetratin and shuffle, indicating a different environment for CF and thus possibly weaker interactions with liposomes in the case of penetramax. 2) At 0.35 mg/mL peptide (0.012 peptide/lipid), the CF fluorescence lifetime distributions (yellow cursors) were shifted toward that of freely diffusing peptides (Fig. 5A). The corresponding pixels are located in the clusters in cases of penetratin and penetramax, while pixels are additionally located outside the clusters in the case of shuffle. 3) At 1.24 mg/mL peptide (0.042 peptide/lipid), the CF fluorescence lifetime distributions (green cursors) were comparable to that of freely diffusing peptides suggestive of excess peptide not interacting with the liposomes. For the peptides in the absence of liposomes, the CF fluorescence lifetime was longer at 0.18 mg/mL peptide compared to that at higher peptide concentrations (Fig. S16B,C). This can be explained by peptide self-assembly, which might influence the peptide-liposome interactions, considering the distinctive lifetime when in the presence of liposomes at the corresponding molar ratio of 0.006 peptide/lipid (Fig. 5A).

To support interpretation of the FLIM data, the fluorescence of the CF-labelled carrier peptides and the effect of liposomes in bulk were investigated by spectroscopy (Fig. 5B). Penetramax was used as a representative peptide for testing the concentration-dependency, while shuffle and penetratin were tested only at low peptide concentrations. At 0.18 mg/mL peptide (0.006 peptide/lipid) in the presence of liposomes, the peak shape was broadened for all three peptides when compared to that of the peptides alone (Fig. 5B). Indeed, this supports the theory of peptide-liposome interactions based on the different fluorescence CF lifetime of peptides alone and in the presence of liposomes (Fig. 5A). Additionally, the peak maximum of the CF-label was slightly shifted towards shorter wavelengths for penetratin and shuffle, but not for penetramax (Fig. 5B), which correlates well with the slightly shorter lifetime of CF-labelled penetramax (Fig. S18). At the higher concentrations of 0.53–1.24 mg/mL penetramax (0.018–0.042 peptide/lipid), the peak shape reverted to the shape of the CF-labelled penetramax alone (Fig. S19).

3.8. Structure of carrier peptides is α-helical in the presence of liposomes

Secondary structure of carrier peptides and the effect of liposomes were investigated by CD (Fig. 5C). At lower peptide concentrations, i.e., 0.006 peptide/lipid, the carrier peptides adopted α-helical structure in the presence of liposomes with the characteristic maximum at 193 nm and minima at 208 and 222 nm [37]. The relative α-helix content was estimated to be 19–29% (Fig. S20C). Signals at 190 nm should be interpreted with caution due to high absorbance values of 1–3 resulting from noise by liposomes and/or high peptide concentrations (Fig. S20A, B). Thus, CD signals at 200–250 nm were used to estimate the relative α-helix and β-sheet contents, where a small normalized root mean square deviation (NRMSD) denote a good fit (Fig. S20C-E). The structure was not well defined for 0.35 mg/mL penetramax (0.012 peptide/lipid) and 0.35–0.53 mg/mL penetratin (0.012–0.018 peptide/lipid) (Fig. 5C), possibly due to the high absorbance (Fig. S20A,B). The carrier peptides unfolded at higher concentrations of 0.88–1.24 mg/mL peptide (0.030–0.042 peptide/lipid) with a CD signal similar to that of the freely diffusing peptide alone in aqueous medium where it was present in a random coil structure with the characteristic minimum at 195 nm and low signal above 210 nm (Fig. 5C, Fig. S21).

3.9. Carrier peptides adsorb to the surface of lipid bilayers

The lifetime of fluorescent dyes is sensitive to environmental parameters and will be distinctive for labelled peptides freely diffusing in aqueous solution compared to labelled peptides associated with liposomes. Based on the applied fluorescence techniques, three key observations were made. 1) The changed CF fluorescence lifetime and 2) the changed CF fluorescence intensity in bulk for peptides in the presence of liposomes compared to that for peptides alone are indicative of interactions between the peptides and the liposomes (Fig. 5A,B). A blue shift of the emission spectra for fluorescein has previously been shown in solvents with increasing hydrogen bonding [38]. The peptides might thus interact with hydrogen bond acceptors, i.e., carbonyl and phosphate groups in the lipid head group rather than with the lipid tails. As hydrogen bond donors, the guanidinium group of arginine forms bidentate hydrogen bonds and has demonstrated stronger interactions with phosphate groups than that of the lysine ammonium group, which forms monodentate hydrogen bonds [39]. This could explain the different peptide-liposome interactions of shuffle when compared to penetramax, despite the subtle difference in the amino acid sequence with substitution of the first and last cationic amino acids (Fig. 1). 3) The unchanged Laurdan fluorescence lifetime for liposomes in the presence of peptides compared to liposomes alone suggests that the membrane fluidity of the liposomes is not changed by the peptides (Fig. 4B). The lifetime of Laurdan-stained liposomes in the form of giant vesicles consisting of 33:67% (mol/mol) POPC:POPG lipids was previously shown to decrease when in presence of the CPP transportan 10 at molar ratios of 0.002–0.009 peptide/lipid, which was caused by insertion into the lipid bilayer [36]. It thus seems plausible that all three carrier peptides investigated in the present study locate at the surface of the liposomes with electrostatic interactions between the peptides and the negatively charged head group of the POPG lipid rather than being located inside the lipid bilayer. Specifically, this is supported by the longer lifetime of the CF-labelled peptides at a low molar ratio of 0.006 peptide/lipid (Fig. 5A; red), which may result from peptide adsorption

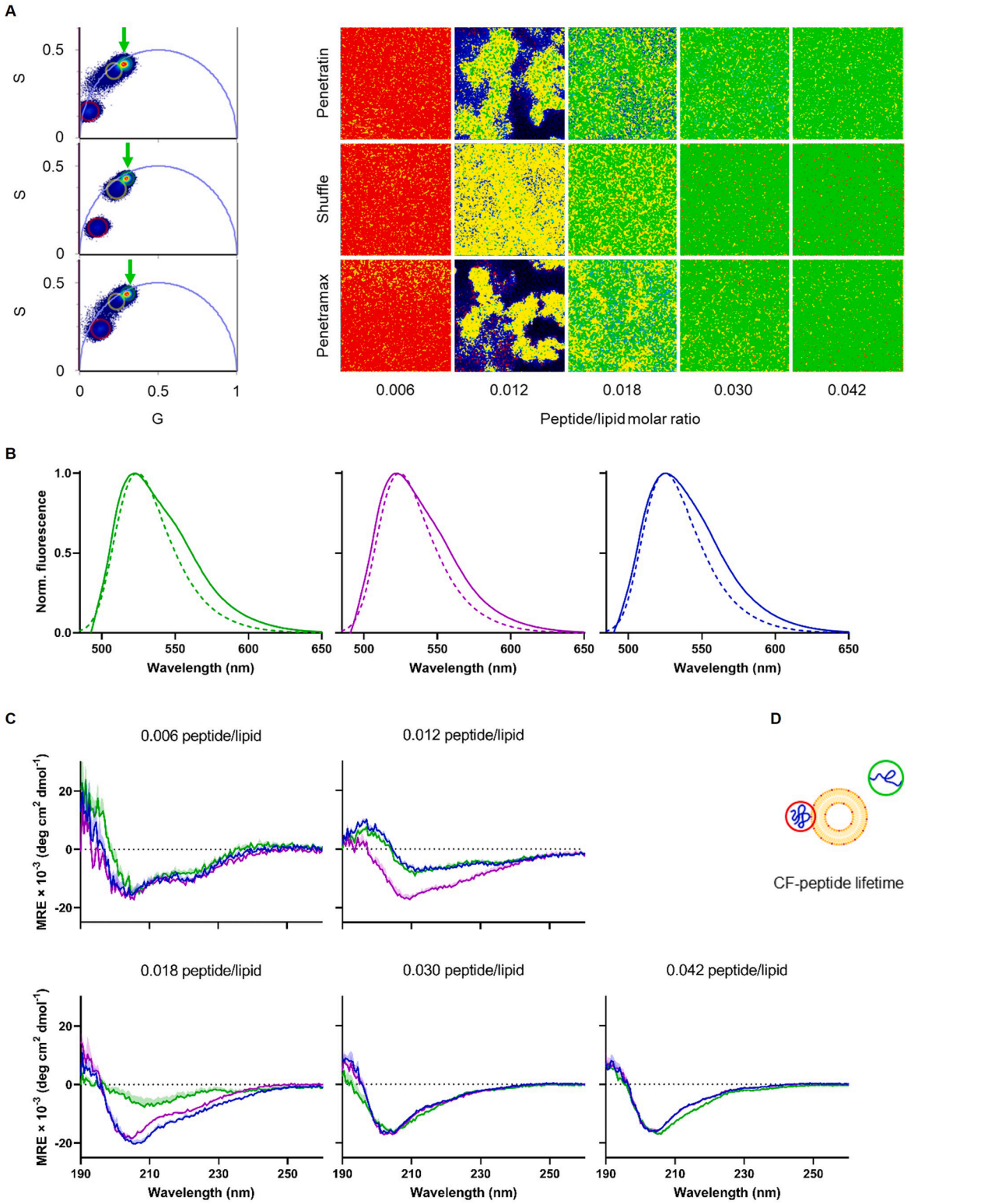

Fig. 5. (A) Representative lifetime displayed in phasor plots, where G and S are phasor vectors (left) and lifetime maps (right) of 0.18 (red circle), 0.35 (yellow circle), 0.53, 0.88, and 1.24 (green circle) mg/mL CF-labelled penetratin (top), shuffle (middle), and penetramax (bottom) in presence of 10 mg/mL Laurdan-stained liposomes consisting of 80:20% (mol/mol) POPC:POPG lipids (0.006–0.042 peptide/lipid) in MES buffer investigated by FLIM (n = 3). The position of the lifetime distribution of 1.24 mg/mL peptide alone is marked with green arrows. (B) Fluorescence intensity of the 0.18 mg/mL CF-labelled penetratin (green), shuffle (purple), and penetramax (blue) in presence of 10 mg/mL liposomes (0.006 peptide/lipid) or the peptides alone (dashed lines) in MES buffer investigated by fluorescence spectroscopy. Mean ± SD (n = 1–3). (A) Secondary structure expressed as mean residue ellipticity (MRE) of 0.18–1.24 mg/mL penetratin (green), shuffle (purple), and penetramax (blue) in the presence of 10 mg/mL liposomes (0.006–0.042 peptide/lipid) in MES buffer investigated by CD. Mean ± SD (n = 5, where n is the number of repeated measurements). (D) Illustration of peptide location relative to lipid bilayer based on lifetime of the CF-label.

to the liposomes, while the lifetime at higher molar ratios (green) results primarily from excess peptides, freely dissolved in the solution as illustrated in Fig. 5D. It has previously been demonstrated possible to distinguish adsorption to the surface from insertion into the bilayer using this technique [40]. Peptide penetration into the lipid bilayer could lead to membrane disruption. The absence of such peptide penetration is thus desirable in regard to the safety profile of the peptides regarding their application as excipient for absorption enhancement for oral delivery of therapeutic peptides. Corroborative to the observations in the present study, other studies have demonstrated relatively low membrane perturbation of penetratin and penetramax [41].

The α-helical structured carrier peptides in the presence of liposomes (Fig. 5C) were previously demonstrated for penetratin in the presence of SDS micelles [8] and liposomes consisting of DOPG lipid [23] and for both penetratin and penetramax in the presence of liposomes consisting of 80:20% (mol/mol) POPC and POPG lipids [41]. This is indicative of association between the peptides and the liposomes. Previously, Persson *et al.* showed presence of β-sheets for penetratin upon liposome aggregation and reversion to α-helices upon the time-sensitive liposome disaggregation after 1.5 h [23]. In the present study, the secondary structure was not well-defined upon liposome clustering, and the random coil structured carrier peptides observed upon reverted liposome clustering are consistent with our previous study at a molar ratio of 0.035 peptide/lipid [2]. The CD signal likely is a merge of a few folded lipid-interacting peptides and many free unfolded peptides in excess. The excess of peptide was confirmed by the increased CF fluorescence intensity in areas without clusters in samples with larger peptide/lipid ratios (Fig. 4A) and by that the fluorescence emission peak reverted at higher penetramax concentrations to that of penetramax alone, i.e., the signal was a result of primarily freely dissolved peptides (Fig. S19).

4. Conclusions

The investigated carrier peptides applied for drug delivery purposes were shown to interact with liposomes primarily by electrostatic interactions resulting in adsorption of the peptides to the surface of the liposome, yet without insertion into the lipid bilayer. The induced liposome clustering by the peptides was reversible and partly reversible at higher peptide/lipid ratios for shuffle and penetramax, respectively, but not for penetratin in the investigated concentration range. This supported that no insertion into the bilayer occurred. Interestingly, however, the liposomes deformed from a spherical to an ellipsoidal shape when shuffle and penetramax adsorbed to their surface. By combining advanced scattering and fluorescence-based experiments with spectroscopy, this study clearly demonstrates that, in addition to the presence of cationic residues, different groupings of uncharged amino acids influence their interactions with membranes as demonstrated by the three different carrier peptides studied. Altogether, detailed understanding of peptide adsorption to membranes and effects hereof applying orthogonal advanced techniques in relation to the peptide sequence generates valuable information for further optimization of peptide-based enhancers. In that regard, reversible peptide interactions with membranes appears favourable for the enhancing properties of the carrier peptides. Further understanding of carrier peptide interactions with membranes would benefit from including more *in vivo* relevant membranes in the biophysical investigation.

CRediT authorship contribution statement

Ragna Guldsmed Diedrichsen: Investigation, Formal analysis, Project administration, Visualization, Writing – original draft. **Valeria Vetri:** Investigation, Formal analysis, Resources, Writing – original draft. **Sylvain Prévost:** Investigation, Formal analysis, Writing – original draft. **Vito Foderà:** Conceptualization, Supervision, Writing – review & editing. **Hanne Mørck Nielsen:** Conceptualization, Resources, Funding acquisition, Supervision, Visualization, Writing – review & editing.

Declaration of Competing Interest

The authors declare that they have no known competing financial interests or personal relationships that could have appeared to influence the work reported in this paper.

Data availability

Data will be made available on request.

Acknowledgements

This project was funded by the Novo Nordisk Foundation (Grand Challenge Programme: NNF16OC0021948 for the Center for Biopharmaceuticals and Biobarriers in Drug Delivery (BioDelivery), University of Copenhagen). V.F. acknowledges VILLUM FONDEN for funding the project via the Villum Young Investigator grant "Protein Superstructures as Smart Biomaterials (ProSmart)" 2018-2023 (19175). This work benefited from the use of the SasView application, originally developed under NSF Award DMR-0520547. SasView also contains code developed with funding from the EU Horizon 2020 programme under the SINE2020 project Grant No 654000. We acknowledge the CFIM (University of Copenhagen) for cryo-TEM. Illustrations were created with icons from BioRender [42].

Appendix A. Supplementary material

Supplementary data to this article can be found online at https://doi.org/10.1016/j.jcis.2023.07.078.

References

[1] E.S. Khafagy, M. Morishita, N. Ida, R. Nishio, K. Isowa, K. Takayama, Structural requirements of penetratin absorption enhancement efficiency for insulin delivery, J. Control. Release. 143 (2010) 302–310, https://doi.org/10.1016/j.jconrel.2010.01.019.

[2] R.G. Diedrichsen, S. Harloff-Helleberg, U. Werner, M. Besenius, E. Leberer, M. Kristensen, H.M. Nielsen, Revealing the importance of carrier-cargo association in delivery of insulin and lipidated insulin, J. Control. Release. 338 (2021) 8–21, https://doi.org/10.1016/j.jconrel.2021.07.030.

[3] A. Walrant, A. Bauzá, C. Girardet, I.D. Alves, S. Lecomte, F. Illien, S. Cardon, N. Chaianantakul, M. Pallerla, F. Burlina, A. Frontera, S. Sagan, Ionpair-π interactions favor cell penetration of arginine/tryptophan-rich cell-penetrating peptides, Biochim. Biophys. Acta, Biomembr. (1862 (2020)), 183098, https://doi.org/10.1016/j.bbamem.2019.183098.

[4] M.-L. Jobin, P. Bonnafous, H. Temsamani, F. Dole, A. Grélard, E.J. Dufourc, I. D. Alves, The enhanced membrane interaction and perturbation of a cell penetrating peptide in the presence of anionic lipids: Toward an understanding of its selectivity for cancer cells, Biochim. Biophys. Acta, Biomembr. 1828 (6) (2013) 1457–1470.

[5] C.Y. Jiao, D. Delaroche, F. Burlina, I.D. Alves, G. Chassaing, S. Sagan, Translocation and endocytosis for cell-penetrating peptide internalization, J. Biol. Chem. 284 (2009) 33957–33965, https://doi.org/10.1074/jbc.M109.056309.

[6] M. Zorko, Ü. Langel, Cell-penetrating peptides, in: Ü. Langel (Ed.), Cell-penetrating peptides: Methods and Protocols, Humana Press, New York, NY, 2022, pp. 3–32, https://doi.org/10.1007/978-1-0716-1752-6_1.

[7] E. Dupont, A. Prochiantz, A. Joliot, Penetratin story: an overview, in: Ü. Langel (Ed.), Cell-Penetrating Peptides: Methods in Molecular Biology, Humana Press, New York, NY, 2015, pp. 29–37, https://doi.org/10.1007/978-1-4939-2806-4_2.

[8] M. Magzoub, K. Kilk, L.E.G. Eriksson, Ü. Langel, A. Gräslund, Interaction and structure induction of cell-penetrating peptides in the presence of phospholipid vesicles, Biochim. Biophys. Acta, Biomembr. 1512 (1) (2001) 77–89.

[9] D. Kalafatovic, E. Giralt, Cell-penetrating peptides: design strategies beyond primary structure and amphipathicity, Molecules. 22 (2017) 1–38, https://doi.org/10.3390/molecules22111929.

[10] R. Gautier, D. Douguet, B. Antonny, G. Drin, HELIQUEST: A web server to screen sequences with specific α-helical properties, Bioinformatics. 24 (2008) 2101–2102, https://doi.org/10.1093/bioinformatics/btn392.

[11] N. Kamei, S. Kikuchi, M. Takeda-Morishita, Y. Terasawa, A. Yasuda, S. Yamamoto, N. Ida, R. Nishio, K. Takayama, Determination of the optimal cell-penetrating peptide sequence for intestinal insulin delivery based on molecular orbital analysis with self-organizing maps, J. Pharm. Sci. 102 (2013) 469–479, https://doi.org/10.1002/jps.23364.

[12] C.N. Pace, F. Vajdos, L. Fee, G. Grimsley, T. Gray, How to measure and predict the molar absorption coefficient of a protein, Protein Sci. 4 (1995) 2411–2423, https://doi.org/10.1002/pro.5560041120.
[13] SasView. http://www.sasview.org/ (accessed January 9, 2021).
[14] A. Guinier, G. Fournet, Small-Angle Scattering of X-Rays, John Wiley and Sons, New York, 1955.
[15] NIST Center for Neutron Research, Neutron activation and scattering calculator, (n.d.). https://www.ncnr.nist.gov/resources/activation/ (accessed January 14, 2021).
[16] T.N. Murugova, P. Balgavý, Molecular volumes of DOPC and DOPS in mixed bilayers of multilamellar vesicles, Phys. Chem. Chem. Phys. 16 (2014) 18211–18216, https://doi.org/10.1039/c4cp01980f.
[17] J. Pan, F.A. Heberle, S. Tristram-Nagle, M. Szymanski, M. Koepfinger, J. Katsaras, N. Kučerka, Molecular structures of fluid phase phosphatidylglycerol bilayers as determined by small angle neutron and X-ray scattering, Biochim. Biophys. Acta, Biomembr. 1818 (9) (2012) 2135–2148.
[18] M.A. Digman, V.R. Caiolfa, M. Zamai, E. Gratton, The phasor approach to fluorescence lifetime imaging analysis, Biophys. J. 94 (2008) L14–L16, https://doi.org/10.1529/biophysj.107.120154.
[19] ISS Inc, Fluorescence lifetime standards, (n.d.). http://www.iss.com/resources/reference/data_tables/FL_LifetimeStandards.html (Accessed November 20, 2021).
[20] D. Magde, G.E. Rojas, P.G. Seybold, Solvent dependence of the fluorescence lifetimes of xanthene dyes, Photochem. Photobiol. 70 (1999) 737–744, https://doi.org/10.1111/j.1751-1097.1999.tb08277.x.
[21] A. Micsonai, F. Wien, L. Kernya, Y.H. Lee, Y. Goto, M. Réfrégiers, J. Kardos, Accurate secondary structure prediction and fold recognition for circular dichroism spectroscopy, Proc. Natl. Acad. Sci. U.S.A. 112 (2015) E3095–E3103, https://doi.org/10.1073/pnas.1500851112.
[22] D. Birch, M.V. Christensen, D. Staerk, H. Franzyk, H.M. Nielsen, Stereochemistry as a determining factor for the effect of a cell-penetrating peptide on cellular viability and epithelial integrity, Biochem. J. 475 (2018) 1773–1788, https://doi.org/10.1042/BCJ20180155.
[23] D. Persson, P.E.G. Thorén, B. Nordén, Penetratin-induced aggregation and subsequent dissociation of negatively charged phospholipid vesicles, FEBS Lett. 505 (2001) 307–312, https://doi.org/10.1016/S0014-5793(01)02843-5.
[24] N. Wichmann, P.M. Lund, M.B. Hansen, C.U. Hjørringgaard, J.B. Larsen, K. Kristensen, T.L. Andresen, J.B. Simonsen, Applying flow cytometry to identify the modes of action of membrane-active peptides in a label-free and high-throughput fashion, Biochim. Biophys. Acta, Biomembr. (1864 (2022)) 1–12, https://doi.org/10.1016/j.bbamem.2021.183820.
[25] O. Maniti, I. Alves, G. Trugnan, J. Ayala-Sanmartin, Distinct behaviour of the homeodomain derived cell penetrating peptide penetratin in interaction with different phospholipids, PLoS One. 5 (2010) e15819.
[26] D. Derossi, A.H. Joliot, G. Chassaing, A. Prochiantz, The third helix of the Antennapedia homeodomain translocates through biological membranes, J. Biol. Chem. 269 (10444–10450) (1994) 10444–10450.
[27] G. Drin, M. Mazel, P. Clair, D. Mathieu, M. Kaczorek, J. Temsamani, Physico-chemical requirements for cellular uptake of pAntp peptide, Eur. J. Biochem. 268 (2001) 1304–1314, https://doi.org/10.1046/j.1432-1327.2001.01997.x.
[28] H.M. Nielsen, K. Browning, H. Chaaban, R.G. Diedrichsen, S. Klodzinska, S. Prevost, Investigating structural organization of cell-penetrating peptides and insulin complexes, in: Institut Laue-Langevin (ILL), Grenoble, 2020. 10.5291/ILL-DATA.9-13-858.
[29] J.E. Nielsen, V.A. Bjørnestad, R. Lund, Resolving the structural interactions between antimicrobial peptides and lipid membranes using small-angle scattering methods: the case of indolicidin, Soft Matter. 14 (2018) 8750–8763, https://doi.org/10.1039/C8SM01888J.
[30] C. Allolio, A. Magarkar, P. Jurkiewicz, K. Baxová, M. Javanainen, P.E. Mason, R. Šachl, M. Cebecauer, M. Hof, D. Horinek, V. Heinz, R. Rachel, C.M. Ziegler, A. Schröfel, P. Jungwirth, Arginine-rich cell-penetrating peptides induce membrane multilamellarity and subsequently enter via formation of a fusion pore, Proc. Natl. Acad. Sci. 115 (2018) 11923–11928, https://doi.org/10.1073/pnas.1811520115.
[31] A. Sauter, F. Zhang, N.K. Szekely, V. Pipich, M. Sztucki, F. Schreiber, Structural evolution of metastable protein aggregates in the presence of trivalent salt studied by (V)SANS and SAXS, J. Phys. Chem. B. 120 (2016) 5564–5571, https://doi.org/10.1021/acs.jpcb.6b03559.
[32] N. Schmidt, A. Mishra, G.H. Lai, G.C.L. Wong, Arginine-rich cell-penetrating peptides, FEBS Lett. 584 (2010) 1806–1813, https://doi.org/10.1016/j.febslet.2009.11.046.
[33] N. Wang, L.D. Clark, Y. Gao, M.M. Kozlov, T. Shemesh, T.A. Rapoport, Mechanism of membrane-curvature generation by ER-tubule shaping proteins, Nat. Commun. 12 (2021) 1–15, https://doi.org/10.1038/s41467-020-20625-y.
[34] O. Golfetto, E. Hinde, E. Gratton, Laurdan fluorescence lifetime discriminates cholesterol content from changes in fluidity in living cell membranes, Biophys. J. 104 (2013) 1238–1247, https://doi.org/10.1016/j.bpj.2012.12.057.
[35] G. Gunther, L. Malacrida, D.M. Jameson, E. Gratton, S.A. Sánchez, LAURDAN since Weber: The quest for visualizing membrane heterogeneity, Acc. Chem. Res. 54 (2021) 976–987, https://doi.org/10.1021/acs.accounts.0c00687.
[36] S. Anselmo, G. Sancataldo, H. Mørck Nielsen, V. Foderà, V. Vetri, Peptide–membrane interactions monitored by fluorescence lifetime imaging: a study case of transportan 10, Langmuir. 37 (2021) 13148–13159, https://doi.org/10.1021/acs.langmuir.1c02392.
[37] N.J. Greenfield, Using circular dichroism spectra to estimate protein secondary structure, Nat. Protoc. 1 (2007) 2876–2890, https://doi.org/10.1038/nprot.2006.202.
[38] M.M. Martin, Hydrogen bond effects on radiationless electronic transitions in xanthene dyes, Chem. Phys. Lett. 35 (1975) 105–111, https://doi.org/10.1016/0009-2614(75)85598-9.
[39] Y. Su, T. Doherty, A.J. Waring, P. Ruchala, M. Hong, Roles of arginine and lysine residues in the translocation of a cell-penetrating peptide from ^{13}C, ^{31}P, and ^{19}F solid-state NMR, Biochem. 48 (2009) 4587–4595, https://doi.org/10.1021/bi900080d.
[40] E. Rao, V. Foderà, M. Leone, V. Vetri, Direct observation of alpha-lactalbumin, adsorption and incorporation into lipid membrane and formation of lipid / protein hybrid structures, Biochim. Biophys. Acta, Gen. Subj. 1863 (5) (2019) 784–794.
[41] S.F. Hedegaard, D.S. Bruhn, H. Khandelia, M. Cárdenas, H.M. Nielsen, Shuffled lipidation pattern and degree of lipidation determines the membrane interaction behavior of a linear cationic membrane-active peptide, J. Colloid Interface Sci. 578 (2020) 584–597, https://doi.org/10.1016/j.jcis.2020.05.121.
[42] BioRender, (n.d.). https://biorender.com/ (Accessed December 19, 2021).